Nuclear Engineering and Technology 53 (2021) 1924–1930

Contents lists available at ScienceDirect

Nuclear Engineering and Technology

journal homepage: www.elsevier.com/locate/net

Original Article

Fracture properties and crack tip constraint quantification of 321/690 dissimilar metal girth welded joints by using miniature SENB specimens

Bao Chen [a, *], Sun Yongduo [b, **], Wu Yuanjun [a], Wang Kaiqing [b], Wang Li [b], He Guangwei [a]

[a] Applied Mechanics and Structure Safety Key Laboratory of Sichuan Province, School of Mechanics and Engineering, Southwest Jiaotong University, Chengdu, 610031, China
[b] Science and Technology on Reactor Fuel and Materials Laboratory, Nuclear Power Institute of China, Chengdu, 610041, China

ARTICLE INFO

Article history:
Received 6 July 2020
Received in revised form
9 December 2020
Accepted 21 December 2020
Available online 28 December 2020

Keywords:
321/690 dissimilar metal girth welded joints
Fracture property
Miniature SENB specimens
Crack tip constraint
J-Q-M approach

ABSTRACT

By using miniature SENB specimens, the fracture properties of the materials in the region of welded metal, 321 stainless steel heat affected zone, 690 alloy heat affected zone of 321/690 dissimilar metal girth welded joints were tested. Both the *J*-resistance curves and critical fracture toughness of the three different materials are affected by the crack size because of the effect of crack tip constraint. Groups of constraint corrected *J*-resistance curves of the three materials are obtained according to *J-Q-M* approach. The welded metals exhibit the best fracture resistance but the worst fracture resistance is observed in the material of 690 alloy heat affected zone.

1. Introduction

The 321/690 dissimilar metal girth welded joint is composed of 321 stainless steel and nickel based 690 alloy. It is commonly used to connect the pipe with pressure vessel in the primary water system of pressurized water reactors. The fracture properties of the girth welded joints play important role in the safety assessment of reactor components. Because of the strength mismatch in the welded metal, heat affected zone of the welded joint, the fracture properties in different region present remarkable difference. It is meaningful to check the fracture properties of the material in the regions of welded metal, 321 heat affected zone and 690 alloy heat affected zone in the laboratory testing. Many researches were made to estimate the fracture properties of dissimilar metal welded joints in nuclear power plant components by using standard compact tension (CT) or single edge notched bending (SENB) specimens [1–12]. Wang and Yang et al. [1–7] used SENB specimen to estimate the fracture toughness of Alloy52 M dissimilar metal welded joint between A508 ferritic steel and 316L stainless steel. Samal et al. [8,9] measured crack tip opening displacement of a dissimilar metal welded joint by using SENB specimens. Brayshaw et al. [10] completed fracture toughness testing on dissimilar metal welded specimens comprised of SA508 Gr.4 N ferritic steel joined to AISI 316L(N) stainless steel via a filler weld of Alloy 82. Laukkanen et al. [11] investigated the fracture properties of dissimilar ferrite SA508-austenite AISI 304 circumferencial weldments by using standard CT specimens. Ogawa et al. [12] conducted the fracture tests by using two types of dissimilar metal weld test plates with semi-elliptical surface crack. As shown in Fig. 1, the base metal 321 stainless steel approaches to the inner edge of the welded joints, while the base metal 690 alloy locates at the outer edge. The width of the welded metal is about 30 mm. It is impossible to extract the standard specimen used for fracture testing from different region of the welded joints because of limit dimensions.

To overcome the limit dimension of the regions of welded metal and heat affected zone, a type of miniature SENB specimen will be used to carry out fracture property tests. It is well known that the fracture toughness of metallic material is commonly affected by the specimen geometry and loading configuration. The difference of

* Corresponding author.
** Corresponding author.
E-mail addresses: bchxx@163.com (B. Chen), 769421283@qq.com (S. Yongduo).

https://doi.org/10.1016/j.net.2020.12.020

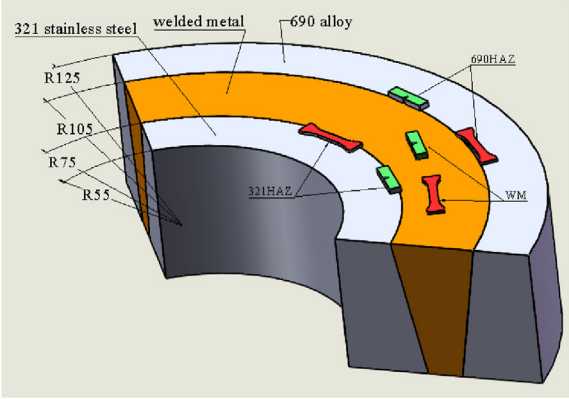

Fig. 1. The configuration of the girth dissimilar metal welded joints and the scheme of sample extraction.

fracture toughness resulted from the different specimen dimension should be quantified. Here, the crack tip constrain principle is capable of dealing with this effect of specimen dimension on the fracture toughness. The crack tip constraint usually includes in-plane and out-of-plane constraints, in which the in-plane constraint correlates to crack size (or remaining ligament size) of specimen, and the out-of-plane is reflected by specimen thickness, but the loading configuration of specimen may affect both the in-plane and out-of-plane constraints. Yang et al. [3,8,11] had investigated the crack tip constraint effect on the local fracture properties of dissimilar metal welded joints. The *J-Q* theory was a classic approach which was widely applied to quantify the in-plane constraint effect on the fracture toughness of materials. O'dowd and Shih [13–15] firstly proposed the *J-Q* approach to eliminate the difference of stress field between HRR solutions and full-field solutions based on finite element analysis. Zhu and Jang [16] found that the original defined parameter *Q* was strongly affected by the loading level, so a load-independent *J-Q* principle was developed. After that, Zhu and Leis [17] proposed a further modified *J-Q* theory to consider the effect of global bending stress on the stress fields ahead of crack tip. Cravero and Ruggieri [18], Pavakumar et al. [19], Wang et al. [20,21] applied *J-Q* theory to estimate the fracture toughness of high pressure pipelines with axial flaws, welded joint with a semi-elliptical crack, respectively. Sometimes, the *J-Q* theory was also approximately used to check the difference of fracture toughness for three dimensional cracks [22–25].

This work will conduct the fracture properties tests on the materials in different regions of 321/690 dissimilar metal girth welded joints using miniature SENB specimens. The effect of crack tip constraint on the fracture toughness of the materials in different regions of the welded joints will be analyzed by using the *J-Q* approach.

2. Materials and experiments

Before the welding operation, the two base metals were machined to have the cross-section configuration as shown in Fig. 1 using wire-cut Electrical Discharge Machining (EDM). Manual backing welding and automatic wire filling welding were carried out to produce the butt joint with a typical single V-groove configuration. The filler wire employed in this study was ERNiCrFe-7A with a diameter of 1 mm.

The chemical compositions (in wt. %) of base metal 321 stainless steel are C 0.062, S < 0.005, Mn 1.41, Si < 0.005, V 0.06, Cr 17.53, Ti 0.5, Cu < 0.08, Co 0.04, P 0.014, B < 0.0005, Ni 10.08, Mo 0.22, W 0.18. The chemical compositions (in wt. %) of base metal 690 alloy are C 28.8, S < 0.0025, Mn 0.2, Si < 0.15, Al 0.24, T 0.23, Fe 9.1, Cu < 0.03, Co < 0.03, P < 0.005, B 0.002, Ni 58.86, As <0.005, Sn < 0.005, Sb < 0.005, Pb < 0.005, H 0.0012, O 0.0072, N 0.0069.

Fig. 2 gives the configuration of the tensile specimens which are used to get uniaxial stress-strain relationship of materials in different regions of the welded joints, such as welded metal (WM), heat affected zone nearing 321 stainless steel (321HAZ), and heat affected zone nearing 690 alloy (690HAZ). As shown in Fig. 1, it is impossible to extract the whole tensile specimen from different region of the welded joints, so the gripped ends by made of universal carbon tool steel are connected to the work zone of the tensile specimen by means of welding.

To investigate the fracture toughness of materials in WA, 321HAZ and 690HAZ regions of the girth welded joints, a special type of miniature SENB specimen was employed in this work, as shown in Fig. 3. The length *L*, width *W*, thickness *B* and net thickness B_N of the SENB specimen are 30 mm, 6 mm, 6 mm, 5 mm, respectively. The crack length *a* is different aiming to check the crack size effect on the fracture toughness. Fig. 1 shows the scheme of extraction of tensile and miniature SENB specimens from different regions of the girth welded joints. 1–3 tensile specimens and 4–7 miniature SENB specimens with different initial crack length have been extracted from each region of the welded joints to measure uniaxial stress-strain curve and fracture toughness, respectively.

Because of the limitation of specimen size, it is impossible to mount the COD (crack opening displacement) extensometer on the miniature SENB specimen. As shown in Fig. 4a), a rigid extended device was designed to measure loading line displacement (LLD) after eliminating the systematic error resulted from the deformation of fixture.

The tensile and fracture toughness tests were carried out on an electromechanical test machine MTS809 with a load frame of 25 kN capacity. The strain of the tensile specimen during loading was measured by using MTS632.29F-30 whose gage length was 5 mm and full strain range was 20%. A standard COD extensometer MTS632.03F-30 with 6 mm gage length and 12 mm full range was mounted on the rigid extended device to measure LLD of the miniature SENB specimen. The scene of fracture toughness testing on the miniature SENB specimen is given in Fig. 4b).

3. Method to the estimation of *J*-resistance curves of welded joints

To estimate *J*-resistance curves of miniature SENB specimens in different regions of the girth welded joints, the load separation-based direct calibration (LSDC) method [26] was applied. Here, the records of load versus LLD for the supposed blunt cracked miniature SENB specimens with different initial crack lengths were obtained by using elasto-plastic finite element analyses based on a 3D finite element model as shown in Fig. 5.

In consideration of the symmetry of specimen geometry and loading configuration, only a quarter of miniature SENB specimen was constructed in commercial code ANSYS 14.5. The indenter and the support of the fixture was set to be rigid by neglecting the

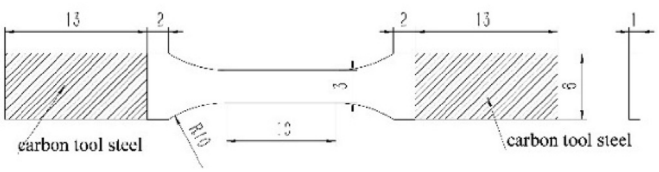

Fig. 2. The configuration of tensile specimen.

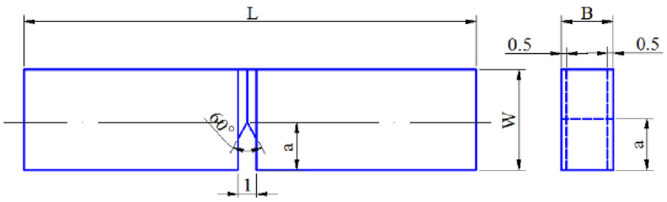

Fig. 3. The configuration of miniature SENB specimen.

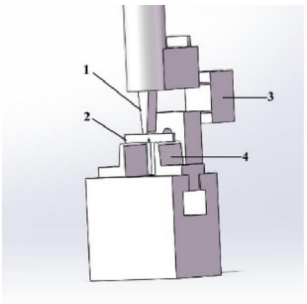

1-indenter 2-specimen 3-COD extensometer 4-support

a) Fixture

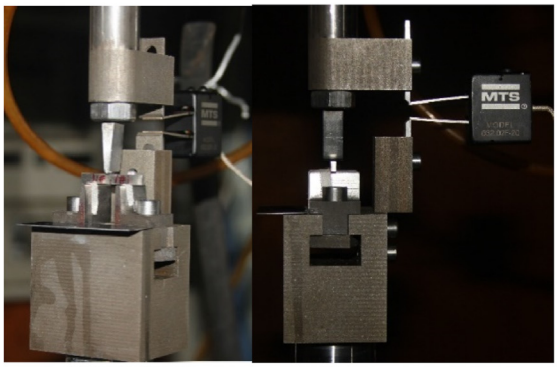

b) The scene of fracture toughness testing on miniature SENB specimen

Fig. 4. Schematic showing of fracture toughness testing on miniature SENB specimen.

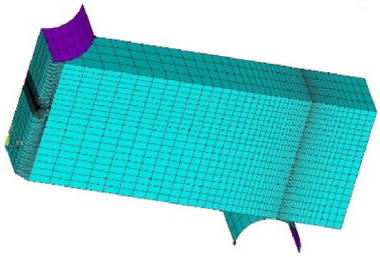

Fig. 5. 3D finite element model of miniature SENB specimen.

deformation of the fixture during loading. The method of rigid-flexible contact analysis was used. A type of Solid185 element was applied to mesh the finite element model, in which the minimum mesh size around the crack tip was 0.2 mm × 0.2 mm × 0.2 mm, and identical planar mesh is repeated along the z-axis from mid-plane ($z/B = 0.5$) to free surface ($z/B = 0$).

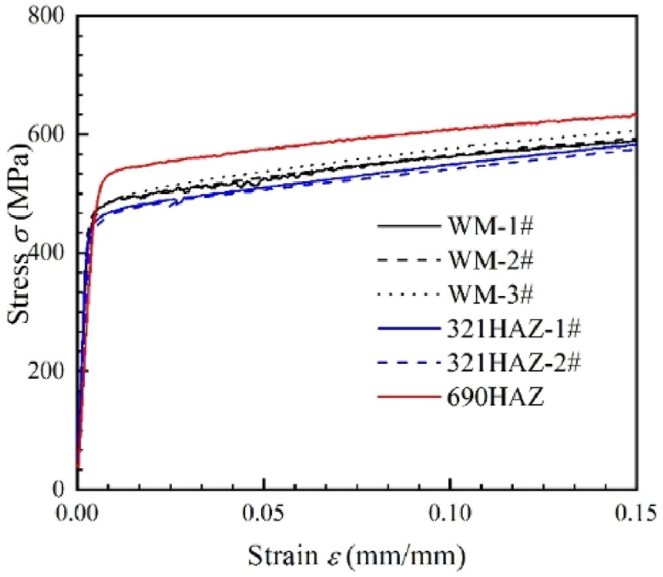

Fig. 6. Uniaxial stress-strain curves of material in different regions of the welded joints.

4. Results and discussion

4.1. Uniaxial stress-strain curves of girth welded joints

Fig. 6 shows the uniaxial stress-strain curves of materials in the three different regions of the girth welded joints. Three specimens in WM region and two specimens in 321 HAZ region were tested. Little data scatter of the specimens extracted from the same region of the welded joints can be observed. The specimen in 690HAZ region presents highest stress-strain curves, while the lowest curve is estimated from the specimen in 321HAZ region. The stress-strain curves of specimens in WM region are a bit higher than those in 321HAZ region. Table 1 lists the tensile properties of materials in the three different regions of the girth welded joints. Because all the stress-strain curves of the welded joints present a character of power strain hardening, so they can be expressed by the typical Ramberg-Osgood model as follows,

$$\frac{\varepsilon}{\varepsilon_0} = \frac{\sigma}{\sigma_0} + \alpha\left(\frac{\sigma}{\sigma_0}\right)^N \tag{1}$$

Where, σ_0 and ε_0 are reference yield stress and strain, α is strain hardening coefficient, N is strain hardening exponent. The parameters of this model for the girth welded joints in different regions are given in Table 1.

4.2. J-resistance curves of the girth welded joints

Figs. 7–9 give the J-resistance curves of the miniature SENB specimens with different initial crack lengths extracted from WM, 321HAZ and 690HAZ regions of the girth welded joints. For the materials in the three different regions of the welded joints, miniature SENB specimens with shallow initial crack length ($a_0/W < 0.3$) and deep initial crack length ($a_0/W > 0.5$) are applied to measure the J-resistance curves. The J-resistance curves of the materials in different regions of the girth welded joints are heavy affected by the crack size. The specimens with shallow crack length

Table 1
Tensile properties of the materials in different regions of the girth welded joints.

Region	WM	321HAZ	690HAZ
Young's modulus/GPa	172	175	106
Yield stress/MPa	475	455	513
Ultimate strength/MPa	645	624	679
ε_0	0.00335	0.00308	0.00562
α	15.271	16.022	6.655
N	4.666	4.527	6.570

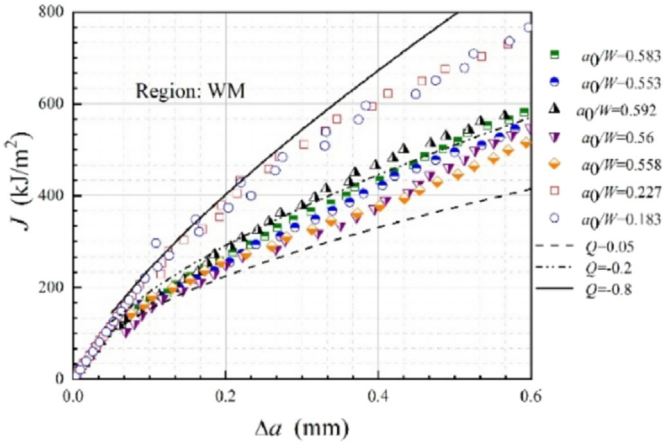

Fig. 7. Experimental and *J-Q-M* approach predicted *J*-resistance curves of the material in WM region of the girth welded joints.

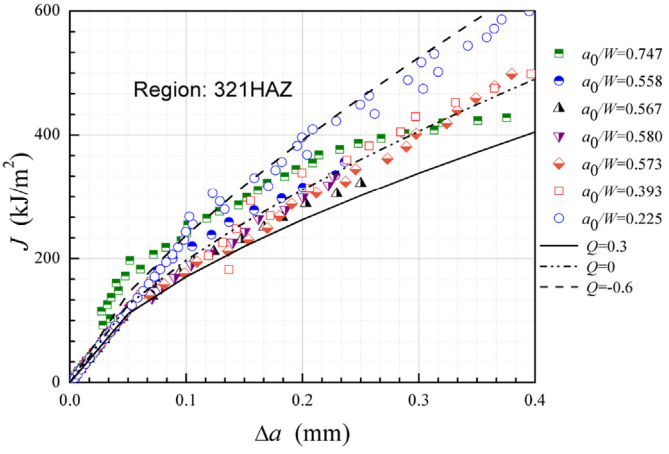

Fig. 8. Experimental and *J-Q-M* approach predicted *J*-resistance curves of the material in 321HAZ region of the girth welded joints.

exhibit higher *J*-resistance curves than those with deep crack length for the materials in WM, 321HAZ and 690HAZ regions of the welded joints.

Table 2 shows the conditional critical fracture toughness J_I and $J_{0.1BL}$ of all the miniature SENB specimens extracted from the four regions of the welded joints. J_I denotes the value of *J*-integral corresponding to the point when the load-displacement curve of tested specimen separating from that of the supposed uncracked specimen because of the occurrence of crack extension. The detailed definition of J_I can be found in the LSDC method [26]. $J_{0.1BL}$ is defined as the intersection of the experimental *J*-resistance curve and the 0.1 mm offset blunting line. The value of J_I is lower than the value of $J_{0.1BL}$ for the same miniature SENB specimen. Both the

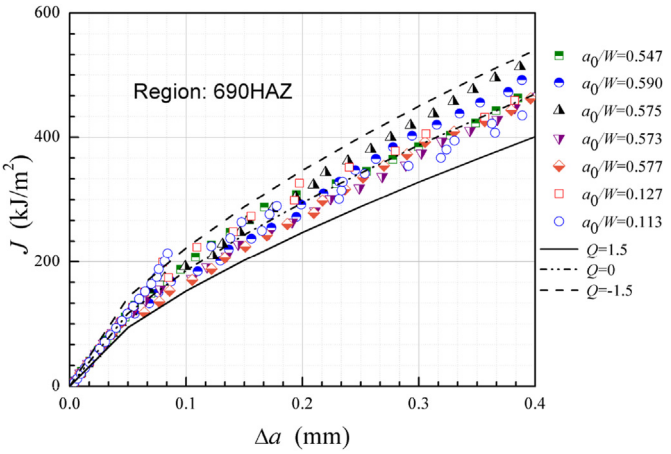

Fig. 9. Experimental and *J-Q-M* approach predicted *J*-resistance curves of the material in 690HAZ region of the girth welded joints.

Table 2
Conditional critical fracture toughness of the welded joints.

Region	a_0/W	J_I /kJ/m²	$J_{0.1BL}$ /kJ/m²	Q
WM	0.583	97.785	279.850	−0.011
	0.553	108.022	269.600	−0.002
	0.592	107.283	320.440	0.066
	0.560	91.409	252.640	−0.052
	0.558	130.242	266.730	−0.183
	0.227	205.904	525.250	−0.472
	0.183	232.238	508.540	−0.621
321HAZ	0.747	73.886	399.870	0.548
	0.558	119.046	358.300	0.151
	0.567	125.653	297.970	0.205
	0.580	121.184	330.180	0.186
	0.573	127.345	334.310	0.129
	0.393	163.196	382.420	−0.029
	0.225	230.324	544.150	−0.495
690HAZ	0.547	135.047	345.350	0.070
	0.590	104.017	356.100	0.200
	0.575	115.324	370.900	0.129
	0.573	106.934	301.460	0.131
	0.577	109.821	292.700	0.140
	0.133	150.810	381.020	−0.859
	0.113	175.151	354.300	−0.962

values of J_I and $J_{0.1BL}$ are obviously affected by the initial crack length of miniature SENB specimens for all the materials in three different regions of the girth welded joints, and the value of J_I is much more sensitive to the crack size effect.

4.3. Discussion on the crack tip constraint of J-resistance curves and critical fracture toughness

4.3.1. Constraint correction of J-resistance curves based on J-Q-M approach

The effect of crack size on the *J*-resistance curves and conditional critical fracture toughness can be explained by the difference of stress state ahead of crack tip according to classic crack tip constraint principle. All the miniature SENB specimens used in this work have the same thickness, so the difference of initial crack size only leads to in-plane crack tip constraint. To quantify the in-plane crack tip constraint on the *J*-resistance curves of the girth welded joints, *J-Q-M* approach will be introduced in the subsequent analysis.

The *J-Q-M* approach dated back to *J-Q* solution [13] and then

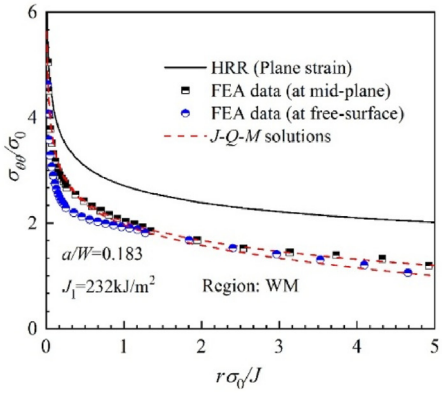

a) Distribution of $\sigma_{\theta\theta}$ along the ligament resulted from FEA and *J-Q-M* solution at θ=0 for miniature SENB specimen in WM region when a/W=0.183, J_I=232kJ/m^2

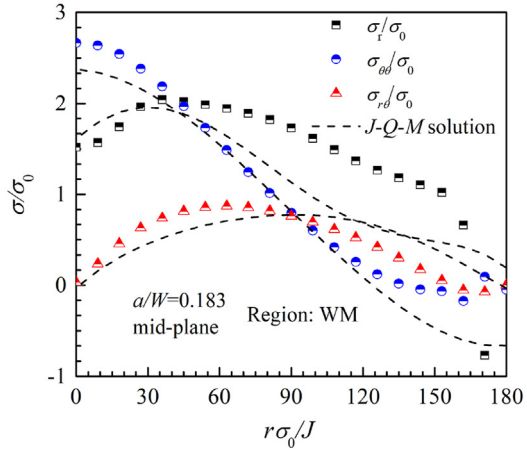

b) Angular distribution of $\sigma_{\theta\theta}$, σ_r, $\sigma_{r\theta}$ at r=0.2mm for miniature SENB specimen in WA region when a/W=0.183, J_I=232kJ/m^2, at mid-plane

Fig. 10. The description of *J-Q-M* solution of crack tip stress fields of miniature SENB specimens in WM region.

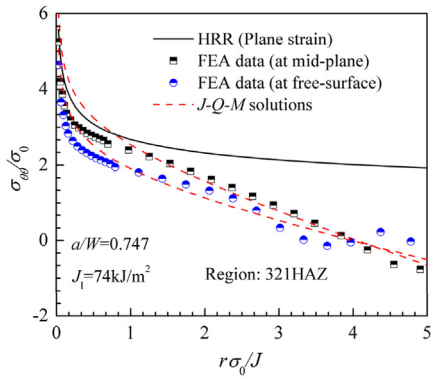

a) Distribution of $\sigma_{\theta\theta}$ along the ligament resulted from FEA and *J-Q-M* solution at θ=0 for miniature SENB specimen in 321HAZ region when a/W=0.747, J_I=74kJ/m^2

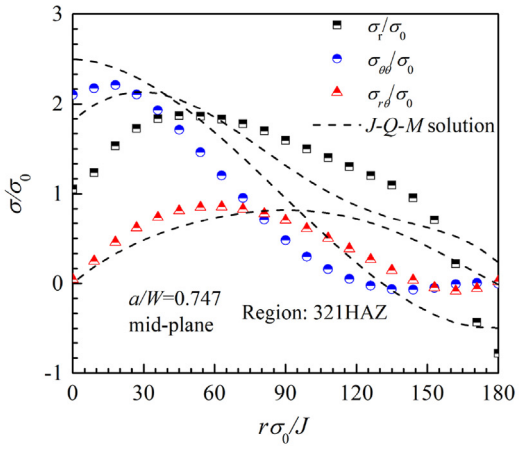

b) Angular distribution of $\sigma_{\theta\theta}$, σ_r, $\sigma_{r\theta}$ at r=0.2mm for miniature SENB specimen in 321HAZ region when a/W=0.747, J_I=74kJ/m^2, at mid-plane

Fig. 11. The description of *J-Q-M* solution of crack tip stress fields of miniature SENB specimens in 321HAZ region.

developed by Zhu and Jang [14] in which a correction term was introduced to eliminate global bending stress effect on the stress fields ahead of crack tip,

$$\frac{\sigma_{\theta\theta}(r,0)}{\sigma_0}=\left(\frac{J}{\alpha\varepsilon_0\sigma_0 I_N k}\right)^{\frac{1}{N+1}}\left[\left(\frac{k}{r}\right)^{\frac{1}{N+1}}\tilde{\sigma}_{\theta\theta}(0,N)+Q\right]+\frac{CMr}{\sigma_0 b^3} \quad (2)$$

where, (r,θ) are the polar coordinates centered at crack-tip, α, N, ε_0, σ_0 are strain hardening coefficient, strain hardening exponent, reference yield strain and reference yield stress of uniaxial stress-strain relationship as described in Eq. (1). $\sigma_{\theta\theta}(r,0)$ is opening stress acting on the crack surface, I_N is an integration constant and $\tilde{\sigma}_{\theta\theta}(0,N)$ is dimensionless stress function. k is a characteristic length and is usually set to be 1 mm. M is resultant bending moment per unit thickness acting on the ligament of specimen and is calculated by the product of load P and width W for miniature SENB specimen. b is the length of remaining ligament of miniature SENB specimen. C is linearization factor and can be explicitly determined by point matching method [27] from Eq. (2) that using two FEA (finite element analysis) estimated opening stress $\sigma_{\theta\theta}^{FEA}(r_1)$ and $\sigma_{\theta\theta}^{FEA}(r_2)$, at two different location $r=r_1$ and $r=r_2$. The constraint parameter Q is finally determined by using weight average method [25].

The numerical simulation of crack tip stress field of the miniature SENB specimen has been carried out by using the finite element model as shown in Fig. 5 in combination with uniaxial stress-strain relationship of the materials in WM, 321HAZ, and 690HAZ regions of the girth welded joints as shown in Fig. 6. Figs. 10–12 schematically show the description of *J-Q-M* solution of crack tip stress fields of miniature SENB specimens in WM, 321HAZ and 690HAZ regions of the girth welded joints. The results show that *J-Q-M* solution match well with the distribution of stress components $\sigma_{\theta\theta}$, σ_r, $\sigma_{r\theta}$ of all the miniature SENB specimens obtained from FEA. The constraint parameters Q for each miniature SENB specimen in different regions of the girth welded joints are given in Table 2.

Based on the *J-Q-M* approach, the constraint corrected *J*-resistance curves can be expressed as,

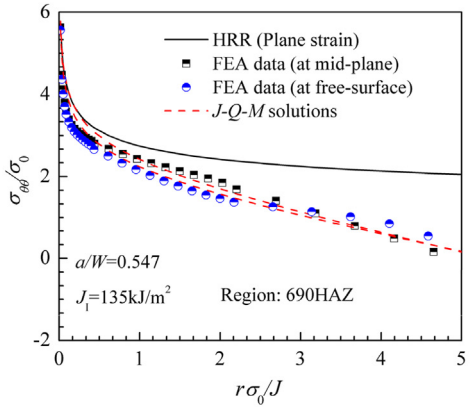

a) Distribution of $\sigma_{\theta\theta}$ along the ligament resulted from FEA and *J-Q-M* solution at θ=0 for miniature SENB specimen in 690HAZ region when a/W=0.547, J_I=135kJ/m^2

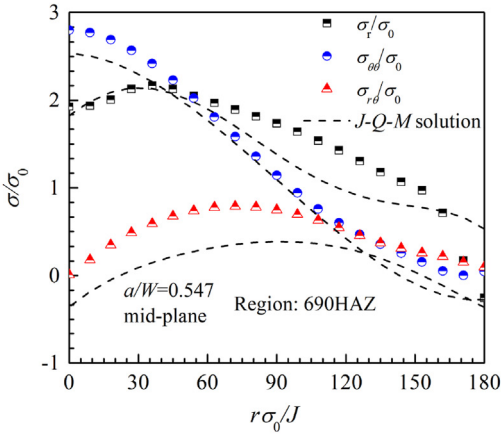

b) Angular distribution of $\sigma_{\theta\theta}$, σ_r, $\sigma_{r\theta}$ at r=0.2mm for miniature SENB specimen in 690HAZ region when a/W=0.547, J_I=135kJ/m^2, at mid-plane

Fig. 12. The description of *J-Q-M* solution of crack tip stress fields of miniature SENB specimens in 690HAZ region.

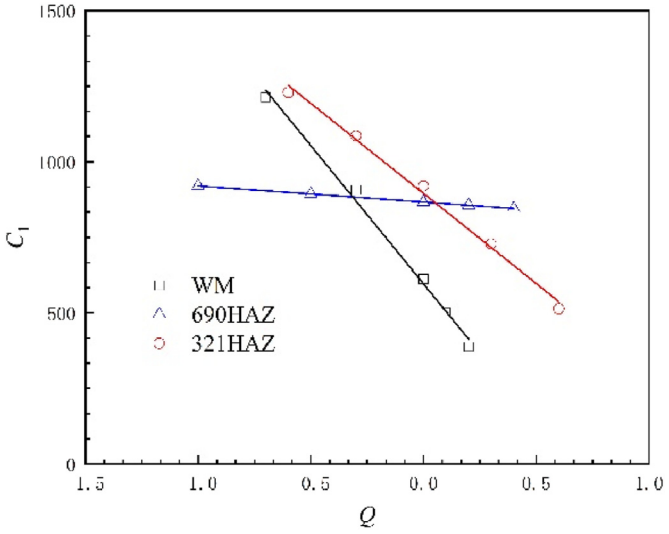

Fig. 13. The relationship of C_1 and Q for the materials in different region.

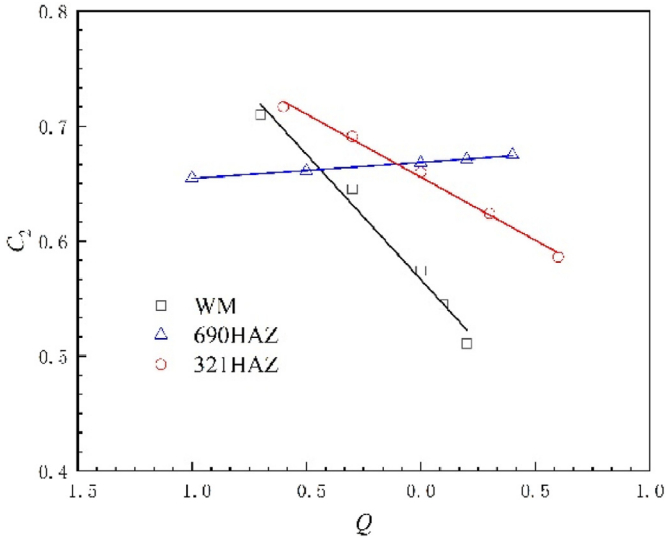

Fig. 14. The relationship of C_2 and Q for the materials in different region.

$$J(\Delta a, Q) = C_1(Q)(\Delta a)^{C_2(Q)} \tag{3}$$

where, $C_1(Q)$ and $C_2(Q)$ are the expression related to the constraint parameters Q. The conditional fracture toughness J_I, $J_{0.1BL}$ listed in Table 2 are used to calibrate the parameters C_1 and C_2. The two parameters can be solved from the relationship of J_I versus Q and the relationship of $J_{0.1BL}$ versus Q as listed in Table 2 using Newton iteration. As seen in Fig. 13 and Fig. 14, the parameters C_1 and C_2 linearly varies with the increase of the constraint parameter Q for all the three materials in WM, 690HAZ and 321HAZ regions. Finally, the constraint corrected *J*-resistance curves are expressed as,

$$J = (d_1 Q + d_2)(\Delta a)^{(d_3 Q + d_4)} \tag{4}$$

The parameters in Eq. (4) for the materials in WM, 321HAZ, and 690HAZ regions of the girth welded joints are listed in Table 3. A family of *J*-resistance curves predicted by Eq. (4) for different crack-tip constraint Q are given in Figs. 7–9. As expected, the lower level

Table 3
The parameters in Eq. (4) for the materials in different regions of the welded joints.

Region	d_1	d_2	d_3	d_4
WM	−914.845	596.080	−0.218	0.567
321HAZ	−595.830	895.139	−0.110	0.656
690HAZ	−53.578	866.488	0.014	0.669

of crack-tip constraint of Miniature SENB specimens presents the higher *J*-resistance curve. The comparison shows that the predicted *J-R* curves from Eq. (4) match well with the experimental data for all specimens. Therefore, Eq. (4) can be effectively used to predict the *J-R* curves for the specimens or actual components of the three materials in different regions of the girth welded joints, if the constraint parameter Q is known.

Based on Eq. (4), a family of *J-R* curves considering constraint

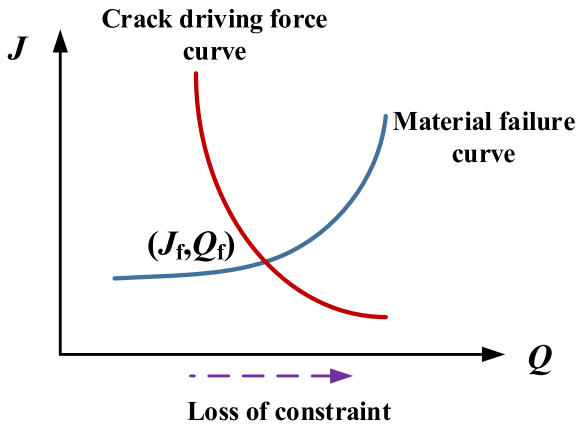

Fig. 15. Schematic showing of fracture failure assessment using *J*-*Q* methodology.

correction for materials in different zone of welded joints can be obtained. On the basis of Table 2, the material failure curve of J_I versus *Q* is determined, as shown in Fig. 15. For a given crack in a service welded structure, perform finite element analysis to determine *J* and *Q* pairs at different loading levels. These data form the crack driving force curve in Fig. 15. Superimpose the material failure curve and crack driving force curve, the failure parameters (J_f, Q_f) can be determined by the point of intersection of the two curves. Consequently, the critical *J*-*R* curve of the service welded structure is estimated by substituting the failure constraint parameter Q_f into Eq. (4).

5. Conclusions

The fracture properties of the materials at WM, 690HAZ and 321HAZ regions of 321/690 dissimilar metal girth welded joints have been tested by using the miniature SENB specimens. The *J*-resistance curves of the three materials in different regions are evidently affected by the crack size. The specimen with shallow crack size presents higher *J*-resistance curves while the lower *J*-resistance curves are given for the specimen with deep crack size. Classic *J*-*Q*-*M* approach is employed to quantify the difference of *J*-resistance curves, then family of constraint corrected *J*-resistance curves of the three materials in different region of the welded joints are obtained. The WM materials present the best fracture resistance but the worst fracture resistance is observed in the materials in 690HAZ. The critical *J*-*R* curve of a given crack in a service welded structure can be estimated by the constraint corrected material failure curves and the crack driving force curve.

Declaration of competing interest

The authors declare that they have no known competing financial interests or personal relationships that could have appeared to influence the work reported in this paper.

Acknowledgement

This work is financially supported by the National Natural Science Foundation of China (Grant No. is 12072294). The authors thank the helpful comments and suggestions from anonymous reviewers.

References

[1] H.T. Wang, G.Z. Wang, F.Z. Xuan, S.T. Tu, An experimental investigation of local fracture resistance and crack growth paths in a dissimilar metal welded joint, Mater. Des. 44 (2013) 179–189.
[2] J. Yang, G.Z. Wang, F.Z. Xuan, S.T. Tu, C.J. Liu, An experimental investigation of in-plane constraint effect on local fracture resistance of a dissimilar metal welded joint, Mater. Des. 53 (2014) 611–619.
[3] H.T. Wang, G.Z. Wang, F.Z. Xuan, S.T. Tu, Fracture mechanism of a dissimilar metal welded joint in nuclear power plant, Eng. Fail. Anal. 28 (2013) 134–148.
[4] J. Yang, L. Wang, Fracture mechanism of cracks in the weakest location of dissimilar metal welded joint under the interaction effect of in-plane and out-of-plane constraints, Eng. Fract. Mech. 192 (2018) 12–23.
[5] K. Fan, G.Z. Wang, F.Z. Xuan, S.T. Tu, Local fracture resistance behavior of interface regions in a dissimilar metal welded joint, Eng. Fract. Mech. 136 (2015) 279–291.
[6] J. Yang, Micromechanical analysis of in-plane constraint effect on local fracture behavior of cracks in the weakest locations of dissimilar metal welded joint, Acta Metall. Sin. 30 (9) (2017) 840–850.
[7] H.T. Wang, G.Z. Wang, F.Z. Xuan, S.T. Tu, Numerical investigation of ductile crack growth behavior in a dissimilar metal welded joint, Nucl. Eng. Des. 241 (2011) 3234–3243.
[8] M.K. Samal, K. Balani, M. Seidenfuss, E. Roos, An experimental and numerical investigation of fracture resistance behavior of a dissimilar metal welded joint, J. Mech. Eng. Sci. 223 (2009) 1507–1523.
[9] M.K. Samal, M. Seidenfuss, E. Roos, K. Balani, Investigation of failure behavior of ferritic-austenitic type of dissimilar steel welded joints, Eng. Fail. Anal. 18 (2011) 999–1008.
[10] W.J. Brayshaw, A.J. Cooper, A.H. Sherry, Assessment of the mirco-mechanical fracture processes within dissimilar metal welds, Eng. Fail. Anal. 97 (2019) 820–835.
[11] A. Laukkanen, Pl Nevasmaa, U. Ehrnsten, R. Rintamaa, Characteristics relevant to ductile failure of bimetallic welds and evaluation of transferability of fracture properties, Nucl. Eng. Des. 237 (2007) 1–15.
[12] T. Ogawa, M. Itatani, T. Saito, T. Hayashi, C. Narazaki, K. Tsuchihashi, Fracture assessment for dissimilar metal weld of low alloy steel and Ni-base alloy, Int. J. Pres. Ves. Pip. 90–91 (2012) 61–68.
[13] N.P. O'Dowd, C.F. Shih, Family of crack-tip fields characterized by a triaxiality parameter-I. Structure of fields, J. Mech. Phys. Solid. 39 (8) (1991) 989–1015.
[14] N.P. O'Dowd, C.F. Shih, Family of crack-tip fields characterized by a triaxiality parameter-II. Fracture Applications, J. Mech. Phys. Solid. 40 (5) (1992) 939–963.
[15] N.P. O'Dowd, Applications of two parameter approaches in elastic plastic fracture mechanics, Eng. Fract. Mech. 52 (3) (1995) 445–465.
[16] X.K. Zhu, S.K. Jang, J-R curves corrected by load-independent constraint parameter in ductile crack growth, Eng. Fract. Mech. 68 (3) (2001) 285–301.
[17] X.K. Zhu, B.N. Leis, Bending modified *J*-*Q* theory and crack-tip constraint quantification, Int. J. Fract. 141 (1–2) (2006) 115–134.
[18] S. Cravero, C. Ruggieri, Correlation of fracture behavior in high pressure pipelines with axial flaws using constraint designed test specimens–Part I: plane-strain analyses, Eng. Fract. Mech. 72 (9) (2005) 1344–1360.
[19] T.V. Pavankumar, J. Chattopadhyay, B.K. Dutta, Numerical investigations of crack-tip constraint parameters in two-dimensional geometries, Int. J. Pres. Ves. Pip. 77 (6) (2000) 345–355.
[20] P. Ding, X. Wang, Solutions of the second elastic plastic fracture mechanics parameter in test specimens under biaxial loading, Int. J. Pres. Ves. Pip. 111–112 (2013) 279–294.
[21] Z.X. Wang, R.F. Zhang, Effect of mechanical property mismatch on failure assessment curve for welded joint with a semi-elliptical crack, Int. J. Appl. Mech. 5 (3) (2013), 1350029(1-18).
[22] V.N. Shlyannikov, N.V. Boychenko, A.V. Tumanov, C.A. Fernandez, The elastic and plastic constraint parameters for three-dimensional problems, Eng. Fract. Mech. 127 (2014) 83–96.
[23] Y. Tkach, F.M. Burdekin, A three-dimensional analysis of fracture mechanics test pieces of different geometries part 2 constraint and material variations, Int. J. Press. Piping 93–94 (2012) 51–56.
[24] X. Wang, G.W. Shen, Three-dimensional finite element analysis of crack-tip fields of clamped single-edge tension specimens-Part II: crack-tip constraints, Eng. Fract. Mech. 116 (2014) 144–157.
[25] C. Bao, L.X. Cai, G.W. He, C. Dan, Normalization method for evaluating J-resistance curves of small-sized CIET specimen and crack front constraints, Int. J. Solid Struct. 94 (2016) 60–75.
[26] C. Bao, L.X. Cai, G.W. He, Y.J. Wu, A method to evaluate ductile fracture toughness based on load separation principle, Fatig. Fract. Eng. Mater. Struct. 42 (1) (2018) 178–186.
[27] Y. Chao, X.K. Zhu, Y. Kim, P. Lar, M. Pechersky, Characterization of crack-tip field and constraint for bending specimens under large-scale yielding, Int. J. Fract. 127 (2004) 283–302.